Validity of Vegard's rule for $Al_{1-x}In_xN$ (0.08<x<0.28) thin films grown on GaN templates

2017 J. Phys. D: Appl. Phys. 50 205107

(http://iopscience.iop.org/0022-3727/50/20/205107)

OPEN ACCESS
IOP Publishing

Made open access 28 June 2017
Journal of Physics D: Applied Physics

J. Phys. D: Appl. Phys. **50** (2017) 205107 (11pp)
https://doi.org/10.1088/1361-6463/aa69dc

Validity of Vegard's rule for $Al_{1-x}In_xN$ ($0.08 < x < 0.28$) thin films grown on GaN templates

S Magalhães[1], N Franco[1], I M Watson[2], R W Martin[3], K P O'Donnell[3], H P D Schenk[4], F Tang[5], T C Sadler[5], M J Kappers[5], R A Oliver[5], T Monteiro[6], T L Martin[7], P A J Bagot[7], M P Moody[7], E Alves[1] and K Lorenz[1]

[1] IPFN, Instituto Superior Técnico, Campus Tecnológico e Nuclear, 2696-953 Sacavém, Portugal
[2] Department of Physics, SUPA, Institute of Photonics, University of Strathclyde, Glasgow, G1 1RD, United Kingdom
[3] Department of Physics, SUPA, University of Strathclyde, Glasgow, G4 0NG, United Kingdom
[4] CNRS-CRHEA, rue Bernard Grégory, 06560 Valbonne, France
[5] Department of Materials Science and Metallurgy, University of Cambridge, Cambridge CB3 0FS, United Kingdom
[6] Departamento de Física e I3N, Universidade de Aveiro, 3810-193 Aveiro, Portugal
[7] Department of Materials, University of Oxford, Oxford OX1 3PH, United Kingdom

E-mail: smagalhães@ctn.tecnico.ulisboa.pt and lorenz@ctn.tecnico.ulisboa.pt

Received 6 February 2017, revised 17 March 2017
Accepted for publication 29 March 2017
Published 28 April 2017

Abstract

In this work, comparative x-ray diffraction (XRD) and Rutherford backscattering spectrometry (RBS) measurements allow a comprehensive characterization of $Al_{1-x}In_xN$ thin films grown on GaN. Within the limits of experimental accuracy, and in the compositional range $0.08 < x < 0.28$, the lattice parameters of the alloys generally obey Vegard's rule, varying linearly with the InN fraction. Results are also consistent with the small deviation from linear behaviour suggested by Darakchieva *et al* (2008 *Appl. Phys. Lett.* **93** 261908). However, unintentional incorporation of Ga, revealed by atom probe tomography (APT) at levels below the detection limit for RBS, may also affect the lattice parameters. Furthermore, in certain samples the compositions determined by XRD and RBS differ significantly. This fact, which was interpreted in earlier publications as an indication of a deviation from Vegard's rule, may rather be ascribed to the influence of defects or impurities on the lattice parameters of the alloy. The wide-ranging set of $Al_{1-x}In_xN$ films studied allowed furthermore a detailed investigation of the composition leading to lattice-matching of $Al_{1-x}In_xN$/GaN bilayers.

Keywords: III-nitrides, AlInN, RBS, XRD, atom probe tomography, Vegard's rule

(Some figures may appear in colour only in the online journal)

1. Introduction

Since the millennium, the optical and electrical properties of III-nitride ternaries ($Al_{1-y}Ga_yN$, $In_yGa_{1-y}N$ and $Al_{1-x}In_xN$) have been explored extensively in the fields of opto- and microelectronics [1]. The band-gap of $Al_{1-x}In_xN$ can, in principle, be tuned from the 0.7 eV of InN to the 6.2 eV of AlN [2], but particular interest focusses on alloys with InN molar fractions around 17–18% which are nearly lattice-matched to GaN. This allows the growth of strain-engineered heterostructures since, in contrast to the cases of $Al_{1-y}Ga_yN$/GaN and $In_yGa_{1-y}N$/GaN, the strain state in $Al_{1-x}In_xN$/GaN can be tuned from tensile to compressive by changing the alloy composition. Furthermore, the growth of low-strain $Al_{1-x}In_xN$/GaN

heterostructures with low densities of strain-induced defects, large band offsets as well as strong polarisation fields promises applications ranging from Bragg mirrors and microcavities [3, 4] to high mobility transistors [5, 6]. $Al_{1-x}In_xN$ can also be used as sacrificial layer for the processing of 3D GaN structures by etching [3, 7].

Because of the large differences in the thermodynamic properties, ionic sizes and ionicity of the constituting binaries, growth of highly crystalline, single-phase $Al_{1-x}In_xN$ in the entire compositional range is challenging. For growth by metal organic chemical vapour deposition (MOCVD), quality quickly deteriorates for InN contents above ~30% due to strain relaxation and phase separation [8, 9]. Ternaries with high InN contents are more readily obtained by low temperature growth techniques such as molecular beam epitaxy (MBE) [10–13] or reactive frequency magnetron sputtering (RFMS) [14–19]. On the other hand, many MOCVD groups have grown high quality $Al_{1-x}In_xN$/GaN in the near-lattice-matched region [3, 8, 20–26].

Despite considerable progress in growing $Al_{1-x}In_xN$/GaN, several fundamental principles are still in dispute. Perhaps the central one is the question of Vegard's rule. Almost a century ago, Vegard stated that, as a rule, the relaxed lattice parameters of a ternary compound can be obtained by linear interpolation between the relaxed lattice parameters of the respective binaries [27]. Corrections to Vegard's rule for the $Al_{1-x}In_xN$ system, adding a bowing parameter to the linear relationship between the lattice parameters, have been proposed on the basis of density functional theory (DFT) calculations [28–30]. Some of the present authors reported experimental evidence of a possible deviation from Vegard's rule, based on a restricted set of samples; the study compared sample compositions measured by x-ray diffraction (XRD) and Rutherford backscattering spectrometry (RBS) [20]. Various works have indicated that the InN content of $Al_{1-x}In_xN$ thin films derived from XRD is likely to be higher than that measured by RBS [14, 20, 31]. However, in some samples the observed deviations are higher than in others. Darakchieva *et al* suggested that *relaxed* $Al_{1-x}In_xN$ follows Vegard's rule while deviations occur for strained layers [31]. Very high discrepancies between compositions measured by XRD and RBS are reported for samples produced by sputtering which cannot be explained by a general deviation from Vegard's rule but suggest instead that high defect densities in these layers introduce hydrostatic strain [14, 19].

In this work, we explore further a possible deviation of Vegard's rule for wurtzite $Al_{1-x}In_xN$ by comparing the composition of a significantly large set of near-lattice-matched $Al_{1-x}In_xN$/GaN bilayers grown in three different MOCVD reactors. Within experimental uncertainty a good agreement between XRD and RBS compositional analysis is found and this agreement is even improved by applying the small modification to Vegard's rule proposed by Darakchieva *et al* [30]:

$$\xi(x) = x\xi^{\mathrm{InN}} + (1-x)\xi^{\mathrm{InN}} + \delta_\xi x(1-x). \qquad (1)$$

with $\xi = a, c$ where $\delta_a = 0.0412 \pm 0.0039$ Å and $\delta_c = -0.060 \pm 0.010$ Å describe bowing parameters for a and c lattice parameters, respectively. However, defects and impurities, in particular unintentional Ga incorporation, will also affect lattice parameters and need to be considered. The implications of Vegard's rule corrections as well as hydrostatic strains on finding the exact lattice-matched composition are discussed.

2. Experimental details

2.1. Sample growth

Three sets of $Al_{1-x}In_xN$/GaN bilayers (C, S and T) were grown by MOCVD using two different close-coupled showerhead reactors (sets C and T) and one horizontal-flow reactor (set S). $Al_{1-x}In_xN$ films with compositions bracketing lattice-match ($0.08 < x < 0.28$) and thicknesses from 20 to 220 nm were mainly grown on GaN buffer layers of ~1–6 μm thickness. All samples were grown under typical MOCVD growth conditions, employing trimethylgallium (TMGa), trimethylindium (TMIn) and trimethylaluminium (TMAl) as metal precursors and ammonia as the group-V precursor. Details have been published previously for series C [22] (10 samples), S [32] (31 samples) and T [21] (10 samples). The majority of the growth templates consisted of GaN/sapphire pre-grown in the same growth reactor as the alloy but the S series includes two samples grown on thick (8–10 μm) commercial GaN-on-sapphire templates, and one on a free-standing GaN substrate, all purchased from Lumilog [33]. Due to the fact that the lattice parameters of these GaN templates all differ from one another, slightly different $Al_{1-x}In_xN$/GaN lattice match conditions are anticipated. It should be noticed that the growth protocol was similar for the three sample sets. First a thin GaN layer was grown at high temperature even when using GaN substrates or GaN/sapphire templates. Then the growth was stopped and the temperature ramped down before starting the $Al_{1-x}In_xN$ growth at lower temperature (around 800 °C).

2.2. Characterization techniques

The $Al_{1-x}In_xN$/GaN samples were analysed using XRD and RBS/Channelling (RBS/C). Chemical composition derived from both techniques was measured in the same region of the sample.

XRD measurements were performed on a Bruker D8 AXS diffractometer. A Göbel mirror, placed in the primary beam path, was used to achieve a parallel beam. The Cu $K_{\alpha 1}$ line was then selected using a 2-bounce Ge (2 2 0) monochromator. To decrease the horizontal angular divergence, a 0.2 mm wide slit was placed between the Göbel mirror and the monochromator collimating the beam to $10 \times 0.2\,\mathrm{mm}^2$. Asymmetric reciprocal space maps (RSM) were acquired using a 0.1 mm slit placed in front of a scintillation detector. Rocking curves (RC) were measured using the open detector.

RBS/C measurements were performed on a Van de Graaff accelerator using a 2 MeV He^+ ion beam of 1 mm diameter. A Si surface barrier detector and a pin diode are placed at backscattering angles of 140° and 165°, respectively, to collect the

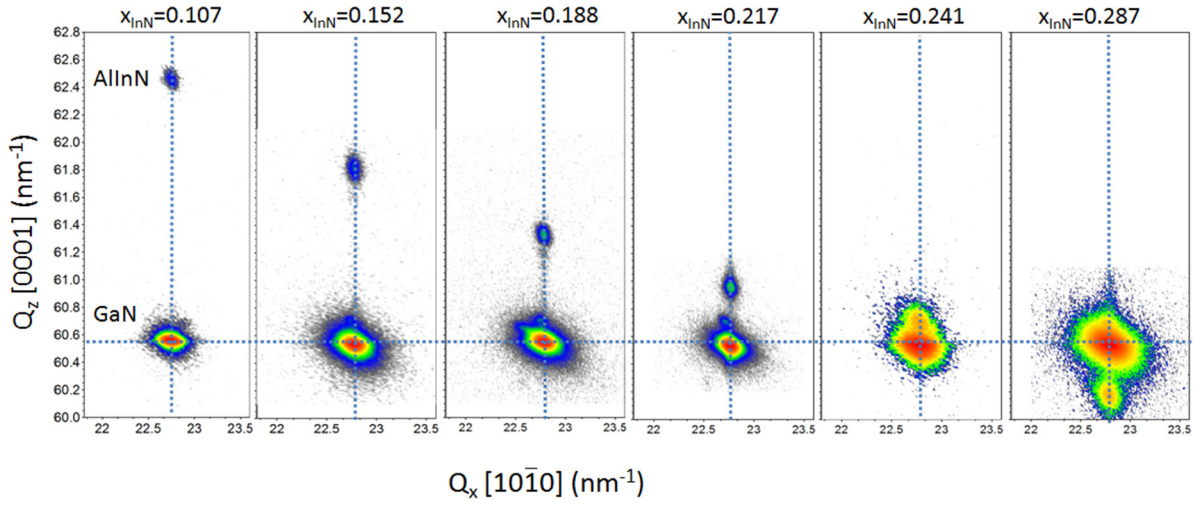

Figure 1. RSM around the $Al_{1-x}In_xN$ and GaN $1\,0\,\bar{1}\,5$ reciprocal lattice points for six representative $Al_{1-x}In_xN$/GaN samples. The InN molar fractions given in the header were determined from the XRD RSM themselves.

backscattered particles. Random RBS spectra were acquired by tilting the surface normal by 5° away from the analysing beam and rotating the sample during the measurement to suppress channelling effects. Compositions and their uncertainties were then derived by careful manual analysis as described in detail in [34]. Furthermore, RBS/C spectra were acquired by aligning the beam with the $\langle 0\,0\,0\,1\rangle$ direction in order to assess the single crystalline quality of the layers.

To facilitate understanding the origin of deviations between XRD and RBS/C compositional analysis, two samples of set C were chosen and studied by atom probe tomography (APT). A local electrode atom probe (LEAP) (CAMECA: 5000XR) was used to examine the $Al_{1-x}In_xN$ layer of sample C1 at a laser pulse energy of 0.02 nJ (UV laser, 355 nm emission wavelength). The $Al_{1-x}In_xN$ layer of sample C2 was studied by a LEAP (CAMECA: 3000X HR) with 0.54 nJ laser energy (Green laser, 532 nm emission wavelength). The LEAP 5000XR has a higher detector efficiency of 0.52, compared to 0.37 for the LEAP 3000X HR, although both instruments are fitted with a reflectron for high resolution mass spectrum analysis. In each APT acquisition, the base temperature of the sample was set at 30 K and evaporation rate was maintained at 0.005–0.01 ions per pulse. APT reconstruction and analysis were carried out using a CAMECA IVAS™ software package calibrated by the thicknesses of $Al_{1-x}In_xN$ layers measured by XRD. APT samples were prepared using a dual beam focussed ion beam based lift-out technique (FEI: Helios NanoLab™) [35].

3. Results and discussion

3.1. Structural characterisation

Representative $(1\,0\,\bar{1}\,5)$ XRD RSM are shown in figure 1 for six $Al_{1-x}In_xN$ ternaries with different compositions. The InN content of these $Al_{1-x}In_xN$ thin films is increasing from left to right as seen by the shifting of the Q_Z peak position, given the known inverse proportionality between Q_Z and c lattice parameter [36]. a and c lattice parameters can then be calculated using the expressions $c = l \cdot 2\pi/Q_Z$ and $a = 2\pi\sqrt{4/3 \cdot (h^2 + k^2)}/Q_X$, with h, k and l being the Miller indices of the measured reflection. According to Vegard's rule, the ternary's c lattice parameter equals that of the GaN buffer layer at approximately 24.7% of InN. In this situation, the XRD peaks of film and template overlap and exact information on composition and crystal quality is difficult to obtain via XRD.

The differences in the a-lattice parameters of the GaN templates and the $Al_{1-x}In_xN$ films extracted from the RSM are typically below 0.002 Å. This difference is similar to the uncertainty of finding the peak position in the maps and shows that that these $Al_{1-x}In_xN$ alloys are pseudomorphic, that is fully strained to the respective GaN templates.

Examples of $(1\,0\,\bar{1}\,4)$ asymmetric and $(0\,0\,0\,4)$ symmetric XRD RCs are shown in figure 2. The full widths at half maximum of the RCs lie between 0.08 ° and 0.15 ° for ternary films of thicknesses in the range between 50 and 160 nm (which is the case for the great majority of the analysed samples) and InN molar fractions between 8% and 28%, revealing a state-of-the-art quality of all samples. The RC FWHM is below 0.07° for all GaN templates. The broadening of the XRD RCs of the ternaries is mainly attributed to the finite film thicknesses and defects. Within the interval studied here, the effect of the composition on the XRD RC broadening can be neglected.

Measuring the RBS/C minimum yield further assesses the crystalline quality. The minimum yield is the ratio between the yield in the aligned spectrum to that of the random RBS yield [37]. Values for pseudomorphic samples ranged from 4% to 10% for the ternary layers indicating a very good and homogeneous crystal quality for the samples used in the compositional analysis.

The morphology and defect type of the three sample sets have been subject of previous investigations [21, 22, 38]. All three sample sets revealed similar features. In fully strained samples, the surface shows typical rms roughness values below 1 nm showing hillocks and V-pits independently of

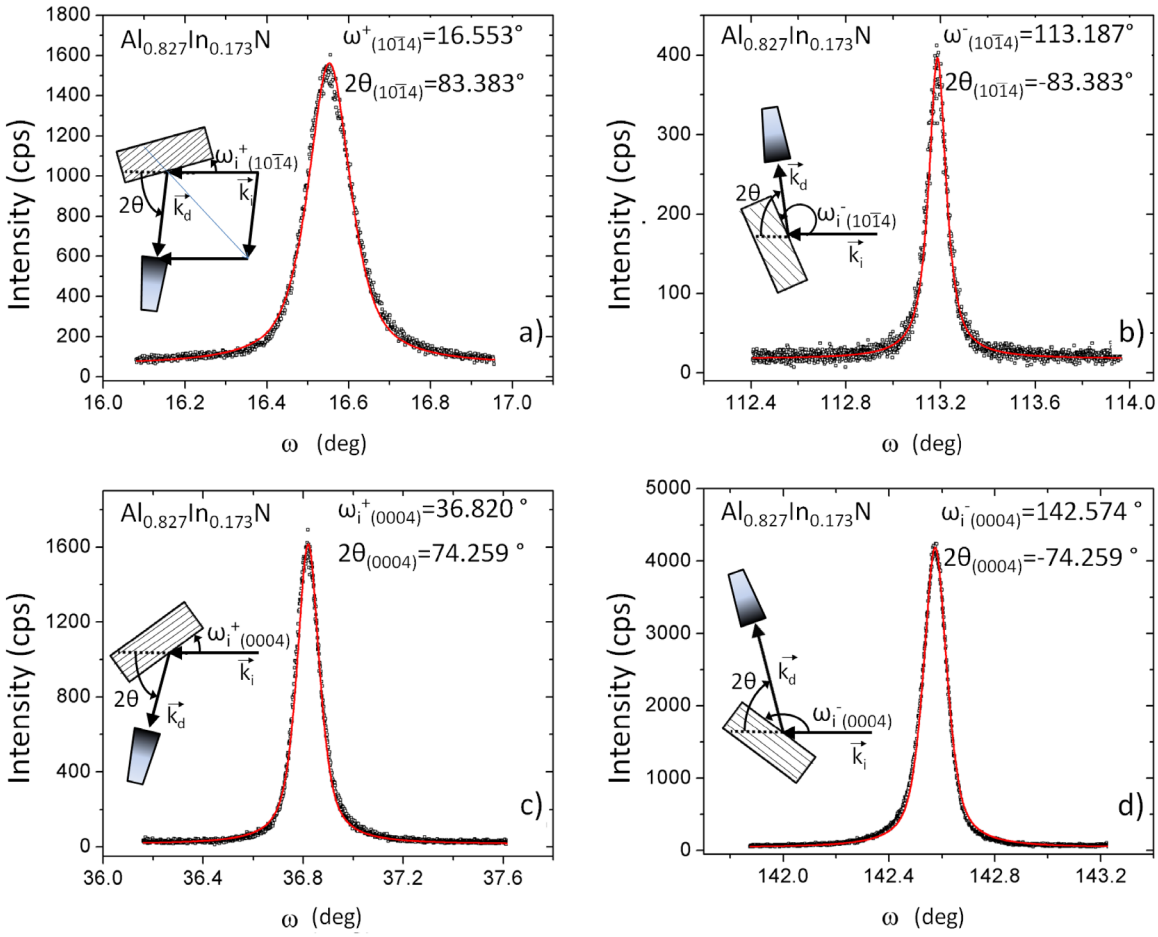

Figure 2. (a)–(d) Experimental XRD RCs of the $(10\bar{1}4^{+}, 10\bar{1}4^{-})$ asymmetric and $(0004^{+}, 0004^{-})$ symmetric reflections (symbols) and fits using a pseudo-Voigt function (solid red lines). The lattice parameters are determined using the measured RC centres and applying the principles from the extended Bond method [40]. The insets show schematics indicating the angle of incidence of the x-ray beam with respect to the sample surface, ω_i. $\vec{k_i}$ and $\vec{k_d}$ are the wave vectors of the incident and diffracted x-ray beam, respectively, and 2θ is the angle between them.

reactor type and layer thickness. Threading dislocations, the dominant defects in III-nitride heterostructures, initiate in the sapphire/GaN interface and cross the entire heterostructure. At the surface they may or may not be terminated by V-pits, depending on the growth conditions [38]. No additional dislocations are formed at the GaN/$Al_{1-x}In_xN$ interface, as expected for near lattice-matched growth. However, the V-pit size increases with layer thickness and overlap of these defects can deteriorate the surface quality [38]. Nevertheless, no macroscopic strain relaxation was measured for the thicker layers analysed in this study, which in fact were all grown with a composition very close to lattice-matching. A small number of samples with very low or very high InN content showed signs of strain relaxation. In particular, tensile strain relaxes via crack formation [22] while compressive strain was shown to lead to surface roughening and sometimes compositional grading [9]. In either case, the relaxation is readily observed in the RSM and these samples were not included in the following study since the resulting asymmetric broadening of XRD curves increases the uncertainty in the XRD compositional analysis, i.e. all samples considered in the following sections are pseudomorphic within experimental accuracy.

Samples with high minimum yield or compositional gradients (evidenced by RBS) were also removed from the study in order to allow an exact evaluation of a possible deviation from Vegard's rule. Accordingly, from a total of 51 samples, 5 were removed.

3.2. Compositional analysis

The procedure to extract the composition of the $Al_{1-x}In_xN$ films and its uncertainty from random RBS spectra by manual analysis has been reported elsewhere [34]. This methodology consists in measuring with high accuracy the In/Al ratio in the film and assuming pure $Al_{1-x}In_xN$ layers without contaminations. The results were confirmed by fitting the RBS spectra using the NDF code [39]. For XRD compositional analysis, a and c lattice parameters were derived for $Al_{1-x}In_xN$ as well as the GaN buffer layer separately by the extended Bond method [40]. For this XRD RCs were acquired using the $(10\bar{1}4^{+}, 10\bar{1}4^{-})$ asymmetric and $(0004^{+}, 0004^{-})$ symmetric reflections. The superscripts denote the position of the x-ray detector with respect to the sample as indicated in the insets of figures 2(a)–(d) which show examples of the experimental

Table 1. Relaxed lattice parameters of the binaries AlN [42] and InN [43] and stiffness coefficients [43, 44] used in this work.

Binary	a_0 (Å)	c_0 (Å)	C_{13} (GPa)	C_{33} (GPa)
AlN	3.111	4.98	99	389
InN	3.537 74	5.7037	121	182

$Al_{1-x}In_xN$ RCs as well as their fits using a Pseudo-Voigt function. The insets show schematics indicating the angle of incidence of the x-ray beam with respect to the sample surface, ω_i. From the relative positions of the $\omega^{\pm}_{i\,0\,0\,0\,4}$ RC centres, the c lattice parameters are derived which are then used together with the $\omega^{\pm}_{i\,1\,0\,\bar{1}\,4}$ RC centres to calculate the a lattice parameters. Consequently the uncertainty in a is higher than that in c. This uncertainty is dominated by the error in finding the centre of each reflection while the effects of mechanical positioning of the goniometer, the x-ray wavelength and correction for refractive index are one order of magnitude lower. The last factor was not considered here. Maximum uncertainties are $\Delta a \sim 0.002$ Å and $\Delta c \sim 0.001$ Å.

To determine the composition, Poisson's equation was used assuming biaxial strain in addition to Vegard's rule [41]. The relaxed a_0 and c_0 lattice parameters of AlN and InN and respective C_{13} and C_{33} stiffness coefficients [42–44] used in this work are listed in table 1.

The presence of biaxial strain leads to a tetragonal distortion of the $Al_{1-x}In_xN$ unit cell. As a consequence, strain also changes the separation of atomic planes. Composition and strain contributions must then be separated by relating the parallel, ε_{xx}, and perpendicular, ε_{zz}, components of the deformation with the elastic constants of the alloy [45]. This is done in terms of the distortion factor D [41]:

$$D = -\frac{\varepsilon_{zz}}{\varepsilon_{xx}} = -\frac{2\upsilon}{1-\upsilon} = -2\frac{C_{13}}{C_{33}} = -\frac{\frac{c_{Al_{1-x}In_xN} - c_0(x)}{c_0(x)}}{\frac{a_{Al_{1-x}In_xN} - a_0(x)}{a_0(x)}}, \qquad (2)$$

where C_{13}, C_{33} are the xz and zz components of the strain tensor, υ is the Poisson ratio, $a/c_{Al_{1-x}In_xN}$ are the measured a/c lattice parameters of the film and $a_0/c_0(x)$ the expected a/c lattice parameters for a relaxed alloy with InN molar fraction x. From equation (2) the following relation between the lattice parameters of a compound, its stiffness coefficients and composition is derived,

$$F(x) = c_{Al_{1-x}In_xN} - \left\{ c_0(x) + 2\frac{c_0(x)}{a_0(x)} \cdot \frac{C_{13}^{Al_{1-x}In_xN}}{C_{33}^{Al_{1-x}In_xN}} \cdot [a_{Al_{1-x}In_xN} - a_0(x)] \right\} = 0, \qquad (3)$$

where the relaxed lattice parameters of the ternaries ($a_0(x)$ and $c_0(x)$) and their stiffness coefficients ($C_{13}^{Al_{1-x}In_xN}$ and $C_{33}^{Al_{1-x}In_xN}$) are calculated by applying Vegard's rule to the reported values of the binaries (table 1). The validity of Vegard's rule for the C_{13} and C_{33} stiffness coefficients has been confirmed by DFT calculations showing approximately linear behaviour [46, 47].

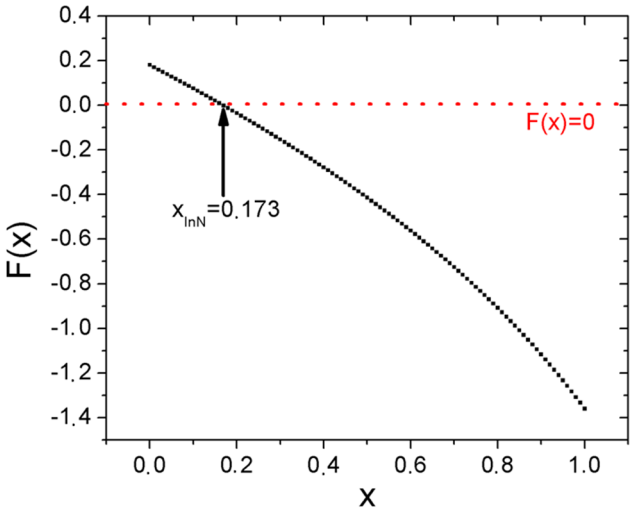

Figure 3. Graphical representation of equation (3) corresponding to a sample with an InN molar fraction of $x = 0.173$.

The solution to equation (3) can be obtained numerically or graphically. Figure 3 represents the function $F(x)$ and confirms that within the region of interest ($0 < x < 1$) this function has only one solution. In this work, a combination of bisection, secant and inverse quadratic interpolation methods was used to solve equation (3) numerically [48]. The uncertainty in the InN molar fraction is then found by deriving the alloy composition for $a \pm \Delta a$ and $c \pm \Delta c$. Thus, the lower and upper bounds on the InN content are obtained and the uncertainty is derived as being half of the difference between these limits leading to maximum values of $\Delta x = 0.002$ for the present sample set.

Figure 4 shows the InN content derived from XRD using either Vegard's rule directly or applying the modification described by equation (1) [30]. The XRD results are plotted against the values measured by RBS for the three sample series. As can be verified from figure 4, for the majority of samples the InN contents derived by XRD (x_{XRD}) using Vegard's rule agree with the values determined by RBS (x_{RBS}) within the uncertainty of the measurements. The uncertainty of $\Delta x \sim 0.002$ maximum in XRD is represented by the height of the symbols. Note that this value only reflects the experimental uncertainty in the determination of the lattice parameters. Systematic errors in the composition determined by XRD will be introduced when using inappropriate values of the materials' parameters summarised in table 1, when further corrections to Vegard's rule are necessary or when hydrostatic strain is present. The uncertainty in x_{RBS} varies from 0.003 for low InN contents to 0.01 for high InN contents with an average of 0.007.

Two samples of set C, sample C1 which shows a good agreement on measured InN composition by RBS and XRD as well as sample C2 with a comparable InN composition but showing a discrepancy between the compositions measured by RBS and XRD, were further analysed by APT. The samples were grown using the same growth protocols but not in consecutive growth runs suggesting that any differences that occur are due to the specific reactor growth history. It is worth noting that APT analysis of the stoichiometry of

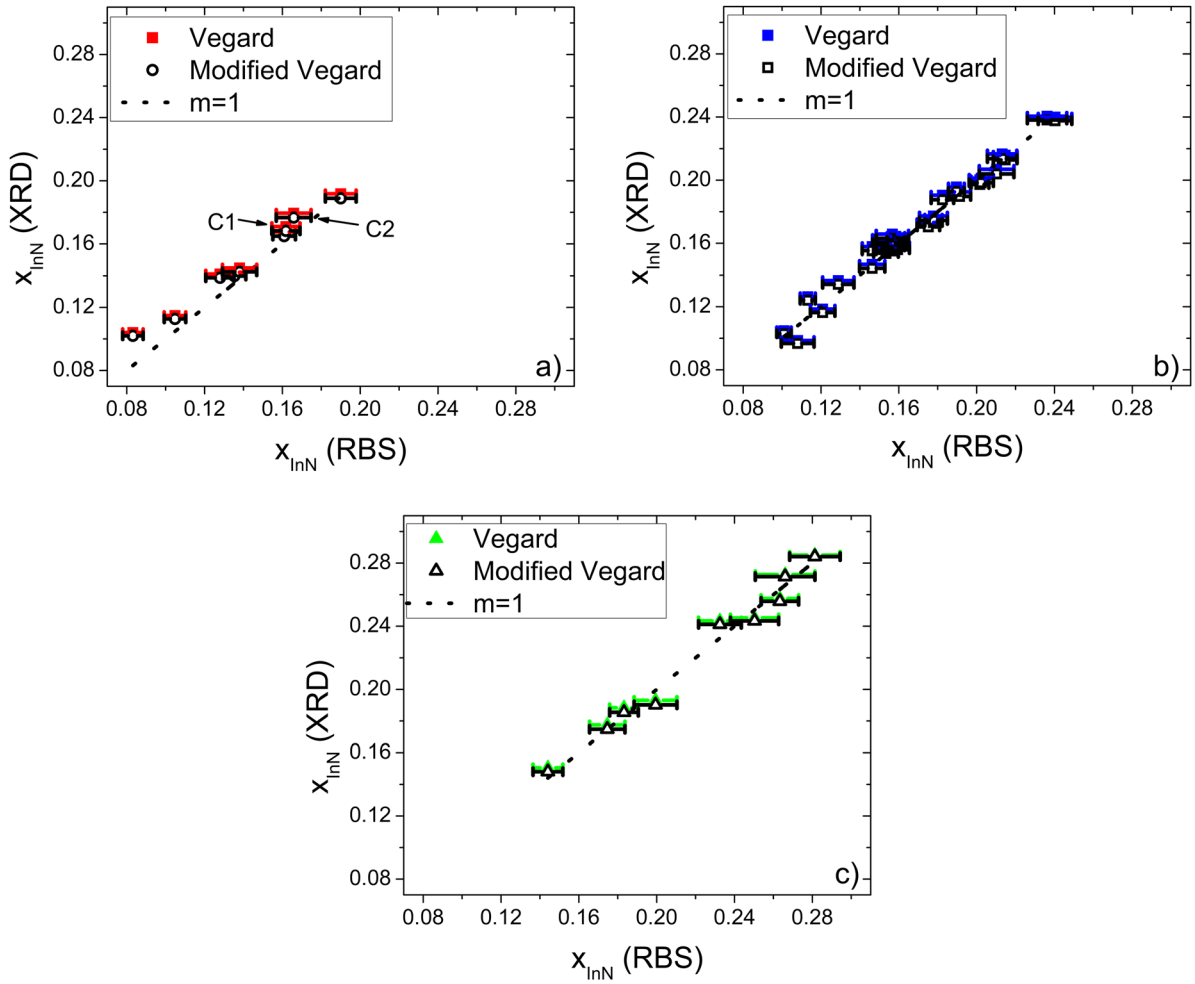

Figure 4. InN content derived from XRD using Vegard's rule [27] or the modified Vegard's rule described by equation (1) [30] as a function of the InN content measured by RBS for sample series C (a), S (b) and T (c). The dashed lines represent the case for which $x_{XRD} = x_{RBS}$. Samples C1 and C2 (marked in (a)) were further analysed by APT.

III-nitride materials is significantly dependent on the parameters used in the APT experiment for reasons which are still under debate [35, 49–52]. Nevertheless, for the analysis of both $In_{1-y}Ga_yN$ and $Al_{1-x}In_xN$, the measured fraction of metallic sites occupied by In atoms has been found to be relatively stable to the running conditions [53]. This is not, however, true of $Al_{1-y}Ga_yN$, where the measured composition has been found to be sensitive to the surface field [54]. The quaternary alloy $Al_{1-x-y}Ga_yIn_xN$ has not been thoroughly studied. For the sake of simplicity, metallic sites, namely In, Al and Ga atoms, were analysed only throughout the APT analysis in this work with the assumption that the group III:group V ratio is stoichiometric, i.e. 1:1, allowing InN, AlN and GaN fractions to be reported.

Figures 5(a) and (c) depict the three-dimensional (3D) distribution of Ga and In atoms in the samples C1 and C2, respectively, where 10% Al iso-concentration surfaces were used to highlight the relative interfaces of $Al_{1-x}In_xN$/GaN layers. It is clear that a considerable amount of incorporated Ga atoms can be observed in $Al_{1-x}In_xN$ layer C2. In contrast, there are only trace levels in C1. Ga distributions in both samples were further quantified using a 'proxigram' (proximity histogram which measures elemental concentration as a function of distance from the GaN/InAlN interface) computed by the 10% Al iso-concentration surface. As shown in figure 5(b), sample C1 presents an abrupt interface and only a slight contamination with 0.4% GaN. On the other hand, for sample C2, a strong Ga-contamination within a thin layer close to the interface with GaN is observed which decreases rapidly towards the surface but remains higher (~1% GaN) than in sample C1.

The average GaN molar fraction in $Al_{1-x}In_xN$ layers is about 0.004 in sample C1 and 0.05 in C2. Table 2 shows the summary of measured compositions of these two samples. It should be pointed out that the compositions in this table measured by APT are the average values so as to compare with the measurements by RBS and XRD. In APT data, several data points towards the exposed $Al_{1-x}In_xN$ surfaces were excluded, since large uncertainties were caused by analysis artefacts associated with very low counts.

These results are consistent with several studies in the literature reporting parasitic Ga-incorporation in $Al_{1-x}In_xN$ layers where the exact Ga-profiles will depend on the history of previous growth runs in the reactor [35, 55–60].

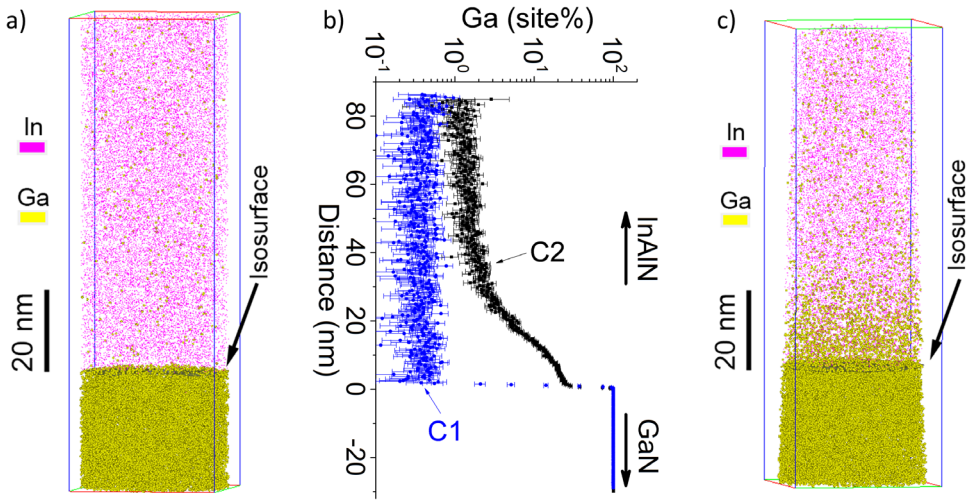

Figure 5. APT analysis of two samples of set C. (a) and (c) 3D images showing reconstructed 10% In atoms and 5% Ga atoms for samples C1 and C2, respectively, where 10% Al iso-concentration surfaces were used to mark the interfaces of $Al_{1-x}In_xN$/GaN. (b) Corresponding Ga profiles of the two samples calculated using a proximity program of 10% Al iso-concentration surfaces.

Table 2. Summary of measured compositions of samples C1 and C2. The number in round bracket shows the uncertainty in the last digit of each measured value. Note that the values for InN (RBS) and InN (XRD) do not take into account systematic errors due to unintentional Ga-incorporation. For the case of APT the results were averaged over the layer thickness in order to allow comparison with the other techniques. The measured *a* and *c* lattice parameters are also given and InN(XRD) was derived using Vegard's rule.

	APT			RBS		XRD		
Sample	GaN	InN	In/Al	InN	In/Al	InN	*a* (Å)	*c* (Å)
C1	0.004 (2)	0.17 (1)	0.21 (1)	0.161 (6)	0.19 (1)	0.168 (2)	3.1845	5.0994
C2	0.05 (1)	0.21 (2)	0.28 (3)	0.166 (9)	0.20 (1)	0.179 (2)	3.1854	5.1119

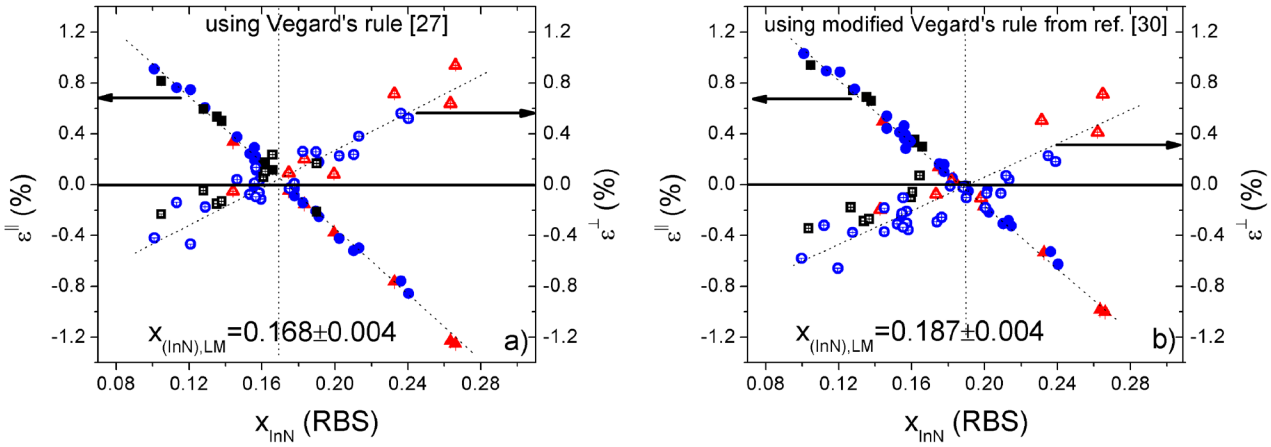

Figure 6. Parallel ($\varepsilon^{\parallel}$) (filled symbols) and perpendicular ($\varepsilon^{\perp}$) (empty symbols) deformations as a function of the RBS InN content using Vegard's rule [27] (a) and the modification of Vegard's rule described by equation (1) [30] (b). Blue circles correspond to series S, black squares to series C and red triangles to series T. Note that both sub-figures correspond to the same RBS and XRD experimental data.

3.3. Strain evaluation

Figure 6 shows the $Al_{1-x}In_xN$ parallel and perpendicular deformations as a function of the InN content measured by RBS.

The lattice-match condition of an $Al_{1-x}In_xN$ film grown on a GaN template is the condition where the film and the template are pseudomorphic, i.e. $a_{\text{film}} - a_{\text{template}} = 0$, and at the same time the deformations parallel ($\varepsilon^{\parallel} = \frac{a_{\text{measured}} - a_0}{a_0}$) and perpendicular ($\varepsilon^{\perp} = \frac{c_{\text{measured}} - c_0}{c_0}$) to the sample surface are zero, that is, the film is relaxed. This condition depends on the composition of the film and on the *a*-parameter of its GaN substrate (or template). Therefore, the lattice-match condition depends on the strain states of the different GaN templates used in this work. For example, GaN grown on *c*-sapphire is usually under compressive strain [61]. Therefore, the film grown on freestanding GaN was not included in figure 6. The differences between the different GaN/sapphire templates prove to be negligible here as can be seen from the fact that the values of $\varepsilon^{\parallel}$ are well described by a linear fit with little

scatter. In fact, the good agreement with the expected linear behaviour confirms that no measurable relaxation takes place. The *a* lattice parameter of a pseudomorphic $Al_{1-x}In_xN$ film is determined solely by the *a* lattice parameter of the GaN template and is unaffected by the eventual presence of hydrostatic strain due to defects. On the contrary, such hydrostatic strains will lead to a variation of the *c* lattice parameter and it is likely that such effects are behind the large scattering of the values for $\varepsilon^{\perp}$ in figure 6. On the other hand, the uncertainty of the RBS measurements will also have an influence via the calculation of the relaxed lattice parameters. Note that this scattering would not be apparent if $\varepsilon^{\perp}$ were to be plotted against x_{XRD} since a variation in *c* lattice parameter is automatically interpreted as a variation in composition and not in hydrostatic strain.

Finally, the lattice-match condition is found by using linear fits of the parallel and perpendicular deformations as a function of the InN content as shown in figure 6 to determine the intersection at $\varepsilon^{||} = \varepsilon^{\perp} = 0$. The uncertainty in the lattice-match InN molar fraction is found using the fit coefficients and their errors. The intersection of the linear fits for parallel and perpendicular deformation yield lattice-match condition for $x_{InN}(LM) = 0.168 \pm 0.004$ when using Vegard's rule (figure 6(a)). Using the modification of Vegard's rule described in equation (1) [30] the lattice match conditions is $x_{InN}(LM) = 0.187 \pm 0.004$ (figure 6(b)).

3.4. Discussion

Good agreement between the composition determined by RBS and XRD is found for 74% of the analysed samples (see figure 4). However, as already observed in previous reports [20, 31], the XRD values tend to exceed the InN molar fractions measured by RBS. In fact, most of the data points in figure 4 lie above the $m = 1$ guide line for which $x_{RBS} = x_{XRD}$ suggesting that, indeed, a correction to Vegard's rule might be required for the $Al_{1-x}In_xN$ alloy. Applying the modification to Vegard's rule described in equation (1) [30], agreement between the two techniques is found for 87% of the measured samples (figure 4). Another indication for a deviation from Vegard's rule is the fact that the interception of the two linear curves for $\varepsilon^{||}$ and $\varepsilon^{\perp}$ in figure 6(a) does not occur at zero but instead at about 0.05%. Again the modification of Vegard's rule [30] does improve these results since the intersection of $\varepsilon^{||}$ and $\varepsilon^{\perp}$ of figure 6(b) occurs practically at $\varepsilon^{||} = \varepsilon^{\perp} = 0$.

Although these findings show that our results are compatible with the proposed modification of Vegard's rule in equation (1) [30], they are no proof since other issues need to be considered. Namely, systematic deviations between the two techniques may alternatively be explained by inadequate values of the relaxed lattice parameters of the binaries or the stiffness coefficients used to determine the composition by XRD. In particular, the InN lattice parameters determined experimentally or theoretically show some dispersion in the literature [43]. The effect of using different published InN lattice parameters from [43] on the InN molar fraction determined by XRD is approximately $\Delta x = 0.002$. In addition to the uncertainty in the binary lattice parameters, tests using the different AlN and InN binary stiffness coefficients reported in [43, 44] also yielded maximum differences on the InN molar fraction of $\Delta x = 0.002$. As an example, we calculated the InN molar fractions using the lattice parameters and stiffness constants recommended by Morales *et al* [62]. The difference between the resultant values for *x* depends on the composition but is below 0.002 for all samples. Although small, this difference raises the fraction of samples agreeing with Vegard's rule from 74% to 78% while when applying the bowing parameters to Vegard's rule the agreement remains at 87% for both sets of materials constants. In conclusion, uncertainties in the lattice parameters and stiffness constants of the binaries have an effect of the same order of magnitude as the modification to Vegard's rule described in equation (1). Note that the errors introduced by incorrect stiffness parameters or bowing can be much higher for the case of semipolar material than for the *c*-plane samples investigated here [47].

Several samples show very high discrepancies between the compositions determined by XRD and RBS. Obviously, these can neither be explained by the uncertainties on Vegard's rule nor on binary parameters, which should of course affect *all* samples. The presence of defects, impurities or microscopic phase separations may explain such large deviations. Indeed, a strong increase of the *c* lattice parameter was observed in GaN upon creation of point defects by particle irradiation [63, 64]. If similar point defects introduce hydrostatic strain during the heterostructure growth, as for example observed for sputter deposited $Al_{1-x}In_xN$ [19], this can explain the overestimation of the InN molar fraction by XRD. In MBE grown $Al_{1-x}In_xN$, discrepancies between the compositions measured by energy dispersive x-ray (EDX) analysis and XRD have been ascribed to a nitrogen deficiency [65]. However, this would lead to a shrinking of the lattice parameters and thus to an underestimation of the InN content, i.e. the opposite of what is observed here.

Within the resolution of the XRD reciprocal space mapping, no macroscopic phase separation was found in the $Al_{1-x}In_xN$ epilayers used in this study. However, microscopic phase separation such as compositional fluctuations or In-clustering may also lead to additional strain in the layer. In fact compositional fluctuations in particular in the vicinity of threading dislocations have been widely reported [66–70].

The samples with highest discrepancy between RBS and XRD composition showed neither wider x-ray RC (as expected for high threading dislocation density) nor higher RBS/C minimum yields for the In-signal (as could be expected for In-clustering). Moreover, no relation between absolute InN content and the observed deviations were found. Further studies are necessary in order to establish the microscopic nature of defects that can cause strong hydrostatic strain in samples with similar structural characteristics. Kaminska *et al* [71] reported a strong fluctuation of the pressure coefficients for $Al_{1-x}In_xN$ alloys with similar composition close to lattice matching in pressure-dependent photoluminescence studies. Possibly such anomalous behaviour can also be explained by hydrostatic strain introduced by defects or by impurities. In particular, Ga contamination features in the literature on MOCVD growth of $Al_{1-x}In_xN$ films [35, 55–60].

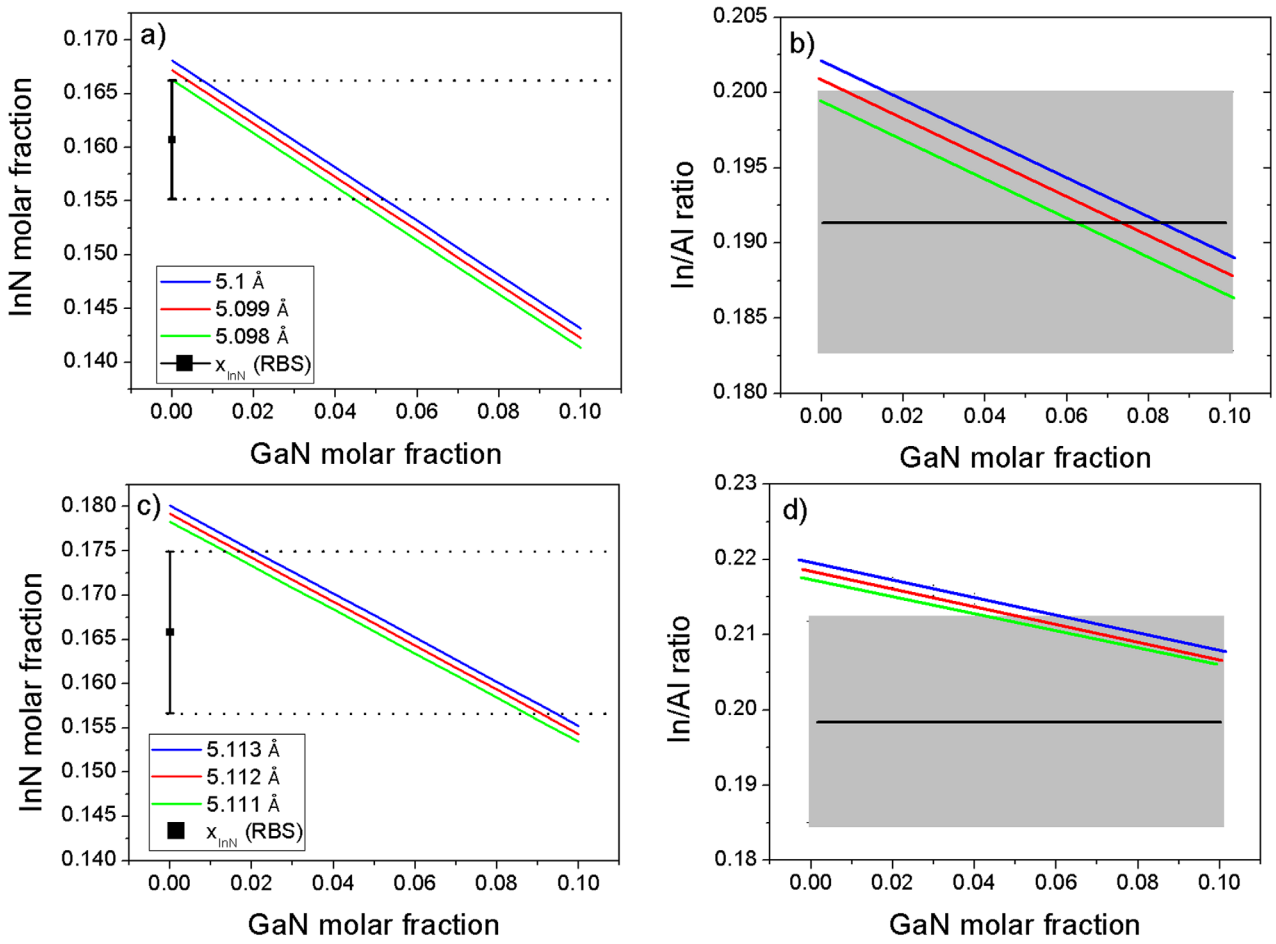

Figure 7. The solid lines in frames (a) and (c) represent all quaternary compositions (up to 10% GaN content) compatible with the measured lattice constants for samples C1 (a) and C2 (c). The central red line corresponds to the measured *c* lattice parameters and the outer lines to the limits defined by the uncertainty of the XRD measurements. The InN molar fraction measured by RBS is also shown (square). Frames (b) and (d) show the In/Al ratio measured by RBS (black horizontal line) and its uncertainty (shaded area) as well as the In/Al ratios compatible with the XRD measurements as a function of GaN incorporation up to 10% (solid coloured lines) for samples C1 (b) and C2 (d).

Kim *et al* [59] attributed unintentional Ga-incorporation to the formation of an eutectic Ga/In liquid formed by the reaction of Ga-containing material deposited on various reactor parts with pyrolized In from injected TMIn. Ammar *et al* [60] showed evidence that unintentional Ga-incorporation is more severe in close-coupled showerhead vertical chambers. In fact, all of the above-mentioned references implicate such reactors. Sample set C, grown in a showerhead reactor, shows a disproportionately high number of samples with discrepant RBS and XRD results.

Incorporation of Ga into $Al_{1-x}In_xN$ while maintaining the In/Al ratio close to the lattice match conditions will lead to an increase of the *c* lattice parameter which can be mis-interpreted as deviations from Vegard's rule since the InN molar fraction will be overestimated when XRD data analysis does not take into account the Ga-contamination.

Although RBS allows a quantitative and depth resolved compositional analysis the sensitivity and depth resolution is limited. In the conditions used for the present analysis we can exclude the incorporation of Ga above ~2% GaN molar fraction in the entire film. For very thin contaminated layers close to the interface to GaN this limit will be higher, thus the Ga-contamination of sample C2 displayed in figure 5(b) could not be resolved in the RBS spectra.

Figure 7 evaluates the effect of such ambiguities for the two samples C1 and C2 with x(RBS) ~ 0.16 where C1 exhibits a good agreement between RBS and XRD (figures 7(a) and (b)) and C2 exhibits a deviation of $\Delta x = 0.013$ (figures 7(c) and (d)).

For the case of quaternaries, equation (3) must be extended by an additional term for GaN when using Vegard's rule to calculate the relaxed lattice parameters and stiffness constants [62]. In fact, for this case the composition is not unambiguously defined by the lattice constants; instead a set of different quaternary compositions can yield the same lattice constants. The lines in figures 7(a) and (c) show all possible compositions of a quaternary film which are compatible with the measured lattice parameters of samples C1 and C2, respectively (the central line corresponds to the measured lattice constant and the outer lines define the error margins of the XRD measurement). The composition determined by RBS and assuming a pure $Al_{1-x}In_xN$ film is also shown (squares). While this composition is inaccurate if Ga-incorporation takes place, the In/Al ratio can be determined with high accuracy from the

RBS spectra since the signals from Al and In are well separated. The horizontal lines and shaded areas in figures 7(b) and (d) correspond to this ratio and its uncertainty, respectively, while the coloured lines mark all possible ratios compatible with the XRD lattice parameter measurements as a function of the GaN-content. It is seen that for sample C1 (figure 7(b)) the In/Al ratio measured by RBS agrees well with all compositions allowed by XRD, i.e. in this sample we cannot exclude the incorporation of Ga to a concentration below the sensitivity limit of RBS of ~2% of GaN. Indeed, APT reveals a low GaN contamination of ~0.4% for this sample while within the uncertainties APT, RBS and XRD results on composition and In/Al ratio agree well. In general we cannot exclude the incorporation of low levels of Ga in samples where XRD and RBS compositions match well.

Figures 7(c) and (d) show a similar analysis for samples with high discrepancies between the composition determined by RBS and XRD using the example of sample C2. Figure 7(d) shows that, for homogeneous samples, unintentional Ga-incorporation can be ruled out as a reason for this discrepancy since the combined RBS and XRD results are not compatible with Ga-incorporation; for low Ga-concentration (<~4 at%) the In/Al ratios do not match while higher Ga-concentrations would be visible in the RBS spectra. However, for the case of sample C2, APT results in figure 5 reveal a strongly inhomogeneous Ga-incorporation in this layer which can likely explain the discrepancies between the three techniques (see table 2). One fact deserves a special note. While the RBS depth resolution is not sufficient to reveal the compositional gradient in this sample, the average In/Al ratio is not affected and should match the APT values. Interestingly, the In/Al ratios measured by RBS and APT in sample C2 differ significantly while they match within uncertainties for sample C1. These results agree with previous works reporting stable APT running condition for $Al_{1-x}In_xN$ [53] but revealing a dependence on the surface field for the case of $Al_{1-y}Ga_yN$ [54]. Further studies are necessary in order to establish stable APT working conditions for quantitative APT analysis in $Al_{1-y}Ga_yN$ and $Al_{1-x-y}Ga_yIn_xN$ quaternary systems.

4. Conclusion

In this work $Al_{1-x}In_xN$ thin films grown in three different reactors (two different close-coupled showerhead reactors and one horizontal-flow reactor) were studied. For 74% of the $Al_{1-x}In_xN$ films, the InN molar fraction from XRD, determined using Vegard's rule, agrees with the RBS results, within the experimental uncertainties. Applying the modification of Vegard's rule described in [30], the agreement increases to 87% of all measured samples indicating that a correction to Vegard's rule does improve consistency. Another indication that the $Al_{1-x}In_xN$ wurtzite system may require Vegard's rule corrections arises from the interpretation of deformation as a function of the ternaries' composition. By comparing the parallel and perpendicular deformations represented as functions of the $Al_{1-x}In_xN$ composition derived by RBS, the intersection between both functions occurs closer to zero deformation if the modified rule is applied. However, the uncertainties of the experimental techniques are too high to allow a definite conclusion or an experimental determination of the bowing parameters to be used in modifying Vegard's rule. In particular, the unintentional incorporation of low concentrations of Ga (<~2 at%) in the films cannot be ruled out. Furthermore, the uncertainties in the binary lattice parameters and stiffness constants introduce further systematic errors in the InN molar fraction determined by XRD of an order of magnitude that is similar to that of the Vegard's rule modification determined in [30].

For routine compositional analysis of $Al_{1-x}In_xN$ by XRD, our study shows that applying Vegard's rule gives acceptably accurate results. However, even small deviation leads to a large difference in the composition leading to lattice-matching with GaN (16.8% using Vegard's rule and 18.7% if applying the modification from [30]). Such a discrepancy may be significant if the exact strain state of a layer needs to be known, for example, when AlInN is used as a sacrificial layer in processing of 3D GaN-based device structures [7]. Strain in such under-etched structures may lead to bending or breaking.

Some of the investigated samples showed significant differences in the derived InN content by both techniques. Such discrepancies may be due to hydrostatic strain due to certain defect configurations or non-random distribution of In. Furthermore, strongly inhomogeneous Ga-incorporation can occur due to Ga-contamination of the growth reactor and complicates compositional analysis.

Acknowledgments

Funding by FCT Portugal grants PTDC/FIS/65233/2006 and PTDC/FIS-NAN/0973/2012 is gratefully acknowledged. SM thanks FCT for his post-doc grant SFRH/BPD/98738/2013 and KL for her grant as 'Investigador FCT'. RAO and FT acknowledge funding from the European Research Council under the European Community's Seventh Framework Programme (FP7/2007-2013)/ERC grant agreement no 279361 (MACONS). The LEAP 5000 XR was funded by the EPSRC grant EP/M022803/1. Deposited experimental data are available via https://pure.strath.ac.uk/portal/

References

[1] Gil B 2013 *Group III Nitride Semiconductors and Their Modern Devices* (*Series of Semiconductor Series and Technology*) (Oxford: Oxford University Press)
[2] Wu J and Walukiewicz W 2003 *Superlatt. Microstruct.* **34** 63–75
[3] Butté R *et al* 2007 *J. Phys. D: Appl. Phys.* **40** 6328–44
[4] Berger C, Dadgar A, Bläsing J, Franke A, Hempel T, Goldhahn R, Christen J and Krost A 2012 *Phys. Status Solidi* c **9** 1253–8
[5] Dadgar A, Schulze F, Bläsing J, Diez A, Krost A, Neuburger M, Kohn E, Daumiller I and Kunze M 2004 *Appl. Phys. Lett.* **85** 5400–2
[6] Gonschorek M, Carlin J-F, Feltin E, Py M A and Grandjean N 2006 *Appl. Phys. Lett.* **89** 062106
[7] Watson I M, Xiong C, Gu E, Dawson M D, Rizzi F, Bejtka K, Edwards P R and Martin R W 2008 *Proc. SPIE* **6993** 69930E

[8] Hums C, Bläsing J, Dadgar A, Diez A, Hempel T, Christen J, Krost A, Lorenz K and Alves E 2007 *Appl. Phys. Lett.* **90** 022105
[9] Lorenz K, Franco N, Alves E, Pereira S, Watson I M, Martin R W and O'Donnell K P 2008 *J. Cryst. Growth* **310** 4058–64
[10] Iliopoulos E, Adikimenakis A, Giesen C, Heuken M and Georgakilas A 2008 *Appl. Phys. Lett.* **92** 191907
[11] Gacevic Z, Garrido S F, Rebled J M, Estrade S, Peiro F and Calleja E 2011 *Appl. Phys. Lett.* **99** 031103
[12] Chen W C, Wu Y H, Peng C Y, Hsiao C N and Chang L 2014 *Nano Scale Res. Lett.* **9** 204
[13] Hardy M T, Storm D F, Nepal N, Katzer D S, Downey B P and Meyer D J 2015 *J. Cryst. Growth* **425** 119–24
[14] Seppänen T, Hultman L, Birch J, Beckers M and Kreissig U 2007 *J. Appl. Phys.* **101** 043519
[15] Guo Q, Tanaka T, Nishio M and Ogawa H 2008 *Japan. J. Appl. Phys.* **47** 612
[16] Afzal N, Devarajan M and Ibrahim K 2015 *Mater. Lett.* **154** 12–6
[17] Han Q, Duan C, Du G, Shi W and Ji L 2010 *J. Electron. Mater.* **39** 489–93
[18] Dong C J, Xu M, Chen Q Y, Liu F S, Zhou H P, Wei Y and Ji H X 2009 *J. Alloys Compounds* **479** 812–5
[19] Hsiao C-L, Palisaitis J, Junaid M, Persson P O Å, Jensen J, Zhao Q-X, Hultman L, Chen Li-C, Chen K-H and Birch J 2012 *Thin Solid Films* **524** 113–20
[20] Lorenz K, Franco N, Alves E, Watson I M, Martin R W and O'Donnell K P 2006 *Phys. Rev. Lett.* **97** 085501
[21] Schenk H P D, Nemoz M, Korytov M, Vennéguès P, Drager A D and Hangleiter A 2008 *Appl. Phys. Lett.* **93** 081116
[22] Sadler T C, Kappers M J and Oliver R A 2009 *J. Cryst. Growth* **311** 3380–5
[23] Buß E R, Rossow U, Bremers H and Hangleiter A 2014 *Appl. Phys. Lett.* **104** 162104
[24] Miyoshi M, Kuraoka Y, Tanaka M and Egawa T 2008 *Appl. Phys. Express* **1** 081102
[25] Lin P-Y, Chen J-Y, Shih Y-S and Chang L 2014 *Nanoscale Res. Lett.* **9** 628
[26] Magalhães S *et al* 2015 *J. Phys. D: Appl. Phys.* **48** 015103
[27] Vegard L 1921 *Z. Phys.* **5** 17–26
[28] Dridi Z, Bouhafs B and Ruterana P 2003 *Semicond. Sci. Technol.* **18** 850–6
[29] Liou B-T, Yen S-H and Kuo Y-K 2005 *Appl. Phys.* A **81** 651–5
[30] Darakchieva V, Xie M-Y, Tasnádi F, Abrikosov I A, Hultman L, Moneman B, Kamimura J and Kishino K 2008 *Appl. Phys. Lett.* **93** 261908
[31] Darakchieva V, Beckers M, Xie M Y, Hultman L, Monemar B, Carlin J F, Feltin E, Gonschorek M and Grandjean N 2008 *J. Appl. Phys.* **103** 103513
[32] Watson I M, Liu C, Dawson M D, Edwards P R and Martin R W 2005 *Appl. Phys. Lett.* **87** 151901
[33] www.ceramicmaterials.saint-gobain.com/lumilog
[34] Magalhães S, Barradas N P, Alves E, Watson I M and Lorenz K 2012 *Nucl. Instrum. Methods Phys. Res.* B **273** 105–8
[35] Tang F, Moody M P, Martin T L, Bagot P A, Kappers M J and Oliver R A 2015 *Microsc. Microanal.* **21** 544–56
[36] Moram M A and Vickers M E 2009 *Rep. Prog. Phys.* **72** 036502
[37] Redondo-Cubero A, Lorenz K, Gago R, Franco N, di Forte Poisson M-A, Alves E and Muñoz E 2010 *J. Phys. D: Appl. Phys.* **43** 055406
[38] Vennéguès P, Diaby B S, Kim-Chauveau H, Bodiou L, Schenk H P D, Frayssinet E, Martin R W and Watson I M 2012 *J. Cryst. Growth* **353** 108–14
[39] Barradas N P *et al* 2008 *Nucl. Instrum. Methods Phys. Res.* B **266** 1338–42
[40] Herres N, Kirste L, Obloh H, Köhler K, Wagner J and Koidl P 2002 *Mater. Sci. Eng.* B **91–2** 425–32
[41] Sadd M H 2004 *Elasticity: Theory, Applications, and Numerics* 1st edn (Burlington: Academic)
[42] Tanaka M, Nakahata H, Sogabe K, Nakata H and Tabioka M 1997 *Japan. J. Appl. Phys.* **36** L1062
[43] Paszkowicz W, Cerny R and Krukowski R 2003 *Powder Diffr.* **18** 114–21
[44] Sheleg A U and Savastenko V A 1979 *Izv. Akad. Nauk SSSR, Neorg. Mater.* **15** 1598–602
[45] Birkholz M, Fewster P F and Genzel C 2006 *Thin Film Analysis by X-Ray Scattering* (Weinheim: Wiley)
[46] Łepkowski S P and Gorczyca I 2011 *Phys. Rev.* B **83** 203201
[47] Xie M Y, Tasnádi F, Abrikosov I A, Hultman L and Darakchieva V 2012 *Phys. Rev.* B **86** 155310
[48] Forsythe G E, Malcolm M A and Moler C B 1976 *Computer Methods for Mathematical Computations* (Upper Saddle River, NJ: Prentice Hall)
[49] Kelly T F, Vella A, Bunton J H, Houard J, Silaeva E P, Bogdanowicz J and Vandervorst W 2014 *Curr. Opin. Solid State Mater. Sci.* **18** 81–9
[50] Dawahre N, Shen G, Renfrow S N, Kim S M and Kung P 2013 *J. Vac. Sci. Technol.* B **31** 041802
[51] Tang F *et al* 2015 *Appl. Phys. Lett.* **106** 072104
[52] Choi S, Wu F, Shivaraman R, Young E C and Speck J S 2012 *Appl. Phys. Lett.* **100** 232102
[53] Mancini L *et al* 2014 *J. Phys. Chem.* C **118** 24136
[54] Rigutti L, Mancini L, Hernández-Maldonado D, Lefebvre W, Giraud E, Butté R, Carlin J F, Grandjean N, Blavette D and Vurpillot F 2016 *J. Appl. Phys.* **119** 105704
[55] Choi S *et al* 2014 *J. Cryst. Growth* **388** 137–42
[56] Kim J *et al* 2014 *J. Cryst. Growth* **388** 143–9
[57] Taylor E, Smith M D, Sadler T C, Lorenz K, Li H N, Alves E, Parbrook P J and Martin R W 2014 *J. Cryst. Growth* **408** 97–101
[58] Smith M D *et al* 2014 *J. Mater. Chem.* C **2** 5787–92
[59] Kim J, Ji M-H, Detchprohm T, Dupuis R D, Fischer A M, Ponce F A and Ryou J-H 2015 *J. Appl. Phys.* **118** 125303
[60] Ammar H B, Minj A, Gamarra P, Lacam C, Tordjman M, di Forte-Poisson M A, Morales M, Chauvat M P and Ruterana P 2016 *Phys. Status Solidi* a **214** 1600441
[61] Zhang L, Shao Y, Hao X, Wu Y, Qu X, Chen X and Xu X 2011 *J. Cryst. Growth* **334** 62–6
[62] Morales F M, Mánuel J M, García R, Reuters B, Kalisch H and Vescan A 2013 *J. Phys. D: Appl. Phys.* **46** 245502
[63] Marques J G, Lorenz K, Franco N and Alves E 2006 *Nucl. Instrum. Methods Phys. Res.* B **249** 358–61
[64] Lorenz K, Peres M, Franco N, Marques J G, Miranda S M C, Magalhães S, Monteiro T, Wesch W, Alves E and Wendler E 2011 *Proc. SPIE* **7940** 79400O
[65] Mánuel J M, Morales F M, Lozano J G, González D, García R, Lim T, Kirste L, Aidam R and Ambacher O 2010 *Acta Mater.* **58** 4120–5
[66] Mouti A, Rouvière J-L, Cantoni M, Carlin J-F, Feltin E, Grandjean N and Stadelmann P 2011 *Phys. Rev.* B **83** 195309
[67] Zhou L, Smith D J, McCartney M R, Katzer D S and Storm D F 2007 *Appl. Phys. Lett.* **90** 081917
[68] Sahonta S-L, Dimitrakopulos G P, Kehagias T, Kioseoglou J, Adikimenakis A, Iliopoulos E, Georgakilas A, Kirmse H, Neumann W and Komminou P 2009 *Appl. Phys. Lett.* **95** 021913
[69] Minj A, Cavalcoli D and Cavallini A 2010 *Appl. Phys. Lett.* **97** 132114
[70] Lei H, Chen J and Ruterana P 2010 *J. Appl. Phys.* **108** 103503
[71] Kaminska A, Nowakowski P, Staszczak G, Suski T, Suchocki A, Carlin J-F, Grandjean N, Martin R and Yamamoto A 2013 *Phys. Status Solidi* b **250** 677–82